Lithos 366–367 (2020) 105544

Contents lists available at ScienceDirect

Lithos

journal homepage: www.elsevier.com/locate/lithos

Research Article

Recycled carbonate-induced oxidization of the convective mantle beneath Jiaodong, Eastern China

Lubing Hong [a,b,*], Yi-Gang Xu [a,c], Le Zhang [a,c], Yu Wang [a,d], Liang Ma [a]

[a] State Key Laboratory of Isotope Geochemistry, Guangzhou Institute of Geochemistry, Chinese Academy of Sciences, Guangzhou 510640, China
[b] College of Earth Sciences, Guilin University of Technology, Guilin 541004, China
[c] School of Earth and Planetary Sciences, University of Chinese Academy of Sciences, Beijing 100049, China
[d] ARC Centre of Excellence for Core to Crust Fluid Systems, NSW 2109, Australia

ARTICLE INFO

Article history:
Received 28 October 2019
Received in revised form 14 April 2020
Accepted 15 April 2020
Available online 20 April 2020

Keywords:
Oxygen fugacity
Olivine
Intraplate basalts
Recycled carbonate
Mantle oxidation
Eastern China

ABSTRACT

The redox state, often expressed as oxygen fugacity (fO_2), is a fundamental parameter controlling geochemical and geodynamic processes. Recent studies have revealed highly variable convective-mantle fO_2 values, but causes of the variability are poorly understood. High fO_2 values of up to 1.6 log units above the Fayalite–Magnetite–Quartz (FMQ) buffer in Cenozoic Jiaodong basalts of eastern China vary as functions of whole-rock and olivine compositions, with strongly alkaline rocks being more oxidized than alkaline varieties, and with the observed fO_2 variations of the basalts most likely reflecting those of the source. Recycled oceanic-crust carbonates occur throughout sources of Cenozoic basalts and may have acted as oxidants in mantle oxidation. We suggest that the melting of a carbonate-bearing peridotite source at depths of ~300 km generated the strongly oxidized alkaline basalts, whereas melting of a pyroxenite source at depths of ~100 km produced the weakly alkaline basalts, with the higher oxidation state of the deeper convective mantle likely resulting from differential melting of various components with unique fO_2 values. This study provides a robust petrological link between mantle oxidation and geochemical recycling, which is key to understanding Earth's evolution and geophysical anomalies in the deep mantle.

1. Introduction

It is widely accepted that redox state in the mantle becomes gradually reduced with increasing depth, due to more ferric Fe substituted into silicate minerals (e.g., Fe^{3+}-rich garnet component; Gudmundsson and Wood, 1995), and redox state in the present-day convective mantle is horizontally relatively homogeneous, as suggested by global mid-ocean-ridge basalts (MORBs) (Bézoes and Humler, 2005; Cottrell and Kelley, 2011). Nonetheless, recent studies have shown highly variable oxygen fugacity (fO_2) values (up to 1.5 log units relative to the Fayalite–Magnetite–Quartz (FMQ) buffer) in the convective mantle horizontally beyond convergent regions (Brounce et al., 2017; Cottrell and Kelly, 2013; Moussallam et al., 2014; Shorttle et al., 2015). Besides, ocean-island basalts (OIBs) are commonly considered as being derived from deeper mantle sources than MORBs (e.g., Niu, 2005) but generally have higher fO_2 values than the latter (Brounce et al., 2017; Moussallam et al., 2014; Nicklas et al., 2019), inconsistent with the general view of redox state in the mantle. The redox state of the convective mantle is thus more complex than previously thought.

Oceanic crust is usually oxidized through hydrothermal reactions (Evans, 2012), and its recycling to Earth's interior is generally considered to be the main convective-mantle oxidation mechanism (e.g., Brounce et al., 2017; Shorttle et al., 2015). However, recycled oceanic crust may be reduced during subduction owing to the release of oxidized hydrous fluids and melts to the mantle wedge (Brounce et al., 2014; Kelley and Cottrell, 2009, 2012). Surface carbon is also delivered to the mantle along with subducted oceanic crust, with most returning to the exosphere through arc volcanism (Evans, 2012; Kelemen and Manning, 2015). Although carbon fluxes in subduction zones are still debated (e.g., Kelemen and Manning, 2015; Hirschmann, 2018), many studies have suggested that appreciable amounts of carbon survive the subduction process (e.g., Kerrick and Connolly, 2001; Li et al., 2017; Hirschmann, 2018). Such recycled carbon, probably in the form of carbonates (Debret et al., 2015), may influence the redox state of the deep mantle (He et al., 2019; Sun and Dasgupta, 2019; Thomson et al., 2016).

The widespread Cenozoic basalts of eastern China occur >1000 km from the western Pacific subduction zone (Fig. 1). These intraplate basalts generally display depleted Nd isotopic and OIB-like trace-element compositions, suggesting an origin in asthenospheric mantle containing recycled oceanic-crust components (Niu, 2005; Xu et al., 2018). Their abnormally low Mg and high Zn isotopic ratios further

* Corresponding author at: State Key Laboratory of Isotope Geochemistry, Guangzhou Institute of Geochemistry, Chinese Academy of Sciences, Guangzhou 510640, China.
E-mail addresses: honglubing@gig.ac.cn, honglubing110320@163.com (L. Hong).

https://doi.org/10.1016/j.lithos.2020.105544
0024-4937/

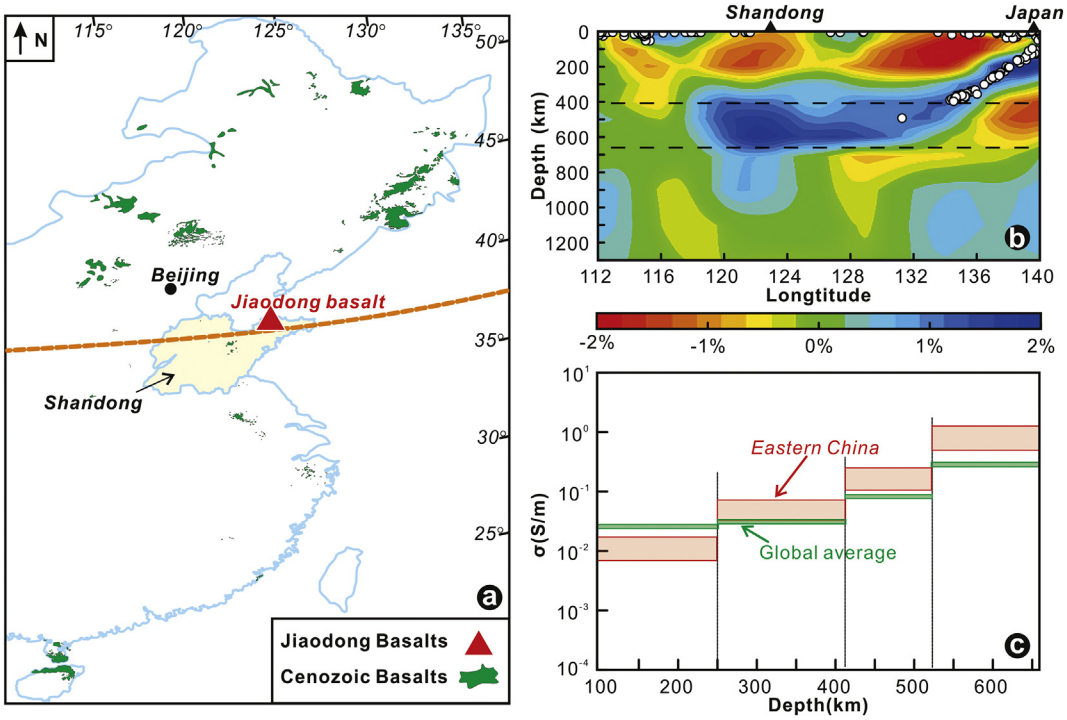

Fig. 1. (a) Simplified geological map of Cenozoic basalt distribution in eastern China. (b) Vertical cross-section of P-wave velocity perturbations along the profile (Huang and Zhao, 2006) shown by the dashed brown line in (a). (c) Comparison of geophysically inferred conductivity (σ)–depth profiles between eastern China and the global average (Karato, 2011).

indicate abundant recycled carbonate in their source (Li et al., 2017; Liu et al., 2016; Wang et al., 2018). The Cenozoic basalts of eastern China thus provide a unique opportunity to solve the enigma of oxidation states in the convective mantle.

Vanadium has three dominant valence states (V^{3+}, V^{4+}, and V^{5+}) with abundances decreasing from V^{3+} to V^{5+}. The crystal–melt V partition coefficient ($D_V^{crystal-melt}$) decreases with increasing fO_2 because of the lower incompatibility of V^{3+} (Canil, 2002). $D_V^{crystal-melt}$ is therefore sensitive to the V oxidation state in the melts, and $D_V^{crystal-melt}$ oxybarometers are widely used to determine fO_2 values of natural magmas (e.g., Canil, 2002; Mallamnn and O'Neill, 2009; Kelley and Cottrell, 2012; Wang et al., 2018). Here, we determined fO_2 values of Cenozoic Jiaodong basalts in Shandong Province, eastern China, by applying the $D_V^{olivine-melt}$ oxybarometry of Canil (2002). Results indicate that recycled carbonate derived from the oceanic crust, rather than recycled oceanic crust, is the main oxidant of convective mantle, and that the higher oxidation states in the deeper convective mantle likely result from the differential melting of various components with unique fO_2 values.

2. Geological background and sample descriptions

Seismic tomography has revealed that the stagnant Pacific Plate extends horizontally to a distance of >1000 km within the mantle transition zone from the western Pacific subduction zone (Fig. 1b; Huang and Zhao, 2006). The mantle beneath this region displays several salient geophysical and geochemical characteristics, including abnormally high electrical conductivity in the mantle transition zone (Fig. 1c; Karato, 2011) and OIB-like geochemical compositions of Cenozoic basalts (Xu et al., 2018) with lighter Mg ($\delta^{26}Mg = -0.6‰$ to $-0.3‰$; Li et al., 2017) but heavier Zn ($\delta^{66}Zn > 0.3‰$; Liu et al., 2016; Wang et al., 2018) isotopic compositions compared with normal mantle ($\delta^{26}Mg = -0.25‰ \pm 0.07‰$; $\delta^{66}Zn = 0.18‰ \pm 0.06‰$; Teng et al., 2010; Wang et al., 2017).

Shandong Province is located on the central coast of eastern China (Fig. 1). Cenozoic basalts that formed there at 24.0–10.3 Ma and 8.7–0.3 Ma (Luo et al., 2009) comprise primarily strongly alkaline basalts (basanite–nephelinite with SiO_2 content <43 wt%) with subordinate weakly alkaline basalts (basaltic andesite–basalt with higher SiO_2 contents; Fig. 2a; Zeng et al., 2010). Detailed geochemical studies of the basalts have revealed large compositional variations, ranging from strongly alkaline basalts with major- and trace-element characteristics of high-U/Pb (HIMU) OIB but with depleted Sr–Nd–Pb–Hf isotopic compositions, to weakly alkaline basalts with enriched-mantle type I (EMI) OIB-like compositions (Zeng et al., 2010; Sakuyama et al., 2013; Li et al., 2016; Fig. 2). Eleven samples were collected from Jiaodong Peninsula, including strongly and weakly alkaline basalts (Table S1; Fig. 2a). All samples have porphyritic texture with large crystals (>200 μm) primarily composed by olivine with minor pyroxene (Fig. 3), suggesting fractionation process is olivine-controlled. Many samples, especially the strongly alkaline basalts, have some (≤6%; Table S1) olivine xenocryts with anhedral corroded outline and embayment (Fig. 3c, d). The samples compositionally cover the range of Shandong basalts (Fig. 2; Table S2).

3. Analytical methods

3.1. Analysis of trace element abundances in whole rocks

Trace element analysis of whole rocks was conducted on Agilent 7700e inductively-coupled plasma mass-spectrometry technique (ICP-MS) at the Wuhan SampleSolution Analytical Technology Co., Ltd., Wuhan, China, following the protocols detailed in Liu et al. (2008).The analytical precision of the procedure based on the two international standard samples (AGV-2 and BHVO-2) are <3% for V and <10% for other elements (Table S3).

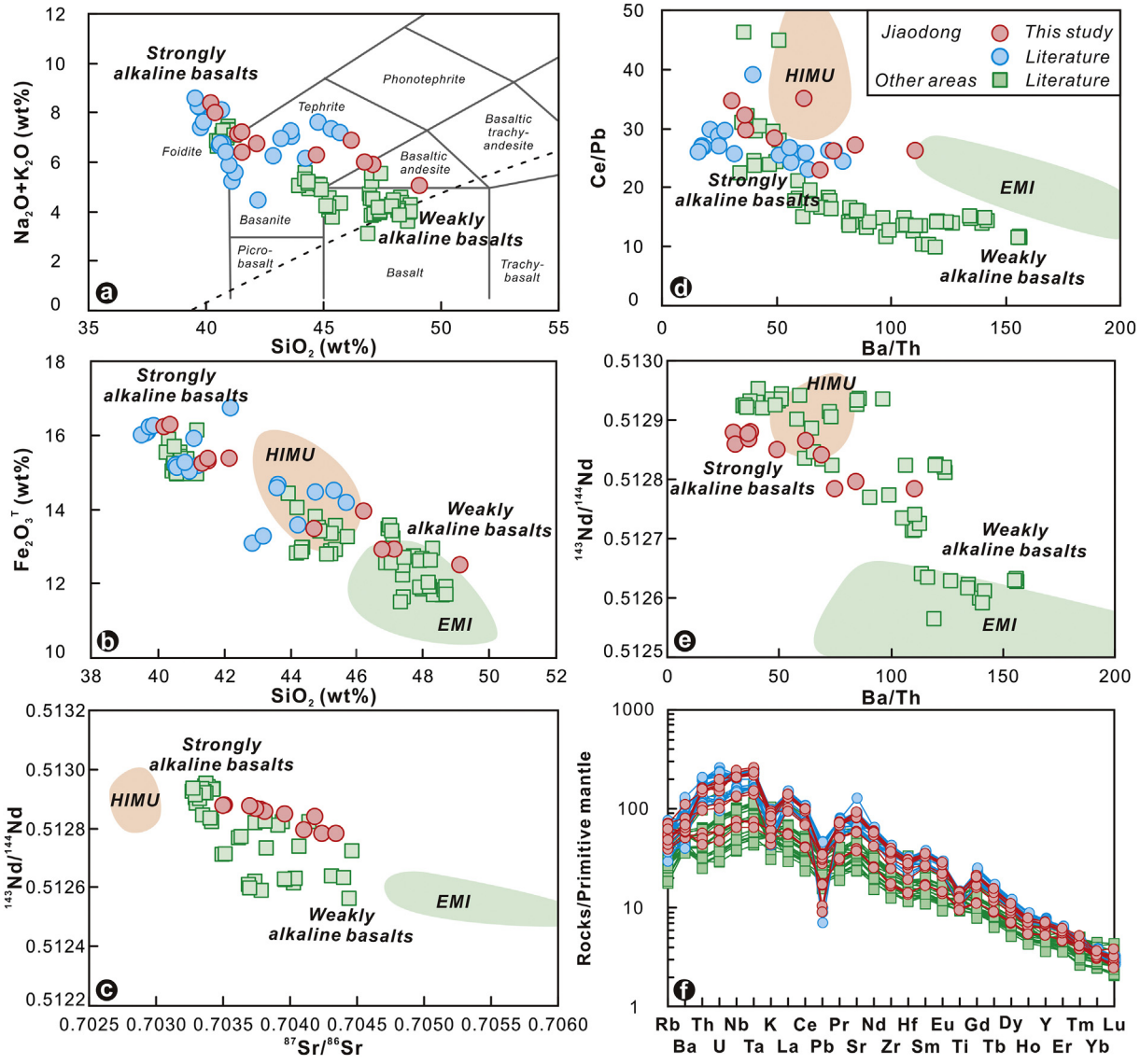

Fig. 2. Plots of whole-rock compositions of the Cenozoic Shandong basalts: (a) ($Na_2O + K_2O$)–SiO_2; (b) $Fe_2O_3^T$–SiO_2, (c) ($^{143}Nd/^{144}Nd$)–($^{87}Sr/^{86}Sr$), (d) (Ce/Pb)–(Ba/Th), (e) ($^{143}Nd/^{144}Nd$)–(Ba/Th), and (f) primitive mantle-normalized spider diagrams. The EMI and HIMU fields were defined by compositional data of typical EMI and HIMU OIBs (http://georoc.mpch-mainz.gwdg.de/georoc/). Compositional data of the Cenozoic Shandong basalts are from Zeng et al. (2010, 2011), Wang et al. (2018), and this study.

3.2. EPMA analysis

The basalts were first crushed, and olivine grains were selected and then mounted in epoxy resin disks. Major element compositions of olivine grains were measured with a JEOL JXA-8100 superprobe at the State Key Laboratory of Isotope Geochemistry, Guangzhou Institute of Geochemistry, Chinese Academy of Sciences (GIG-CAS). The operating conditions were as follows: 15 kV accelerating voltage, 20 nA beam current and 1 μm beam diameter, and 10s peak counting time for major elements (Mg, Fe, Si) and 40s peak counting time for Ca. The reduction was carried out using ZAF correction.

3.3. LA-ICP-MS analysis

The same olivine grains were analyzed for trace element by in situ laser ablation-inductively coupled plasma-sector field-mass spectrometry (LA-ICP-SF-MS) at the State Key Laboratory of Isotope Geochemistry, GIG-CAS. Detailed operating conditions for the laser ablation system and the ICP-MS instrument in the LA-ICP-SF-MS analysis are the same as described by Zhang et al. (2019). Analyses were carried out with helium as a carrier gas and argon as the make-up gas. The spot size and frequency of the laser were set to 33 μm and 5 Hz, respectively. Olivine compositions were calibrated against three reference materials (BHVO-2G, BCR-2G and GSD-1G) with Mg as an internal standard. Each analysis included a 20 s background acquisition and a 30 s data acquisition. Two international reference materials (TB-1G and BIR-1G) were measured during the analytical procedure. A MATLAB program named TraceElement was used to perform an off-line selection, the integration of background and analyzed signals, and a quantitative calibration for the analysis (Zhang et al., 2019). The relative accuracy and precision of the TB-1G and BIR-1G are better than 10% for the key elements (Table S4). A single crystal of San Carlos olivine ($Fo_{90.8}$) was also analyzed periodically to determine the uncertainties of V in the olivines usually with V < 10 ppm, and the reproducibility between replicate spots was within 5% relative standard deviation. On the basis of the ~5% uncertainty in the V content (2.87 ppm) of a San Carlos olivine standard, the analytical uncertainty in ΔFMQ values is estimated to be <0.13 log units.

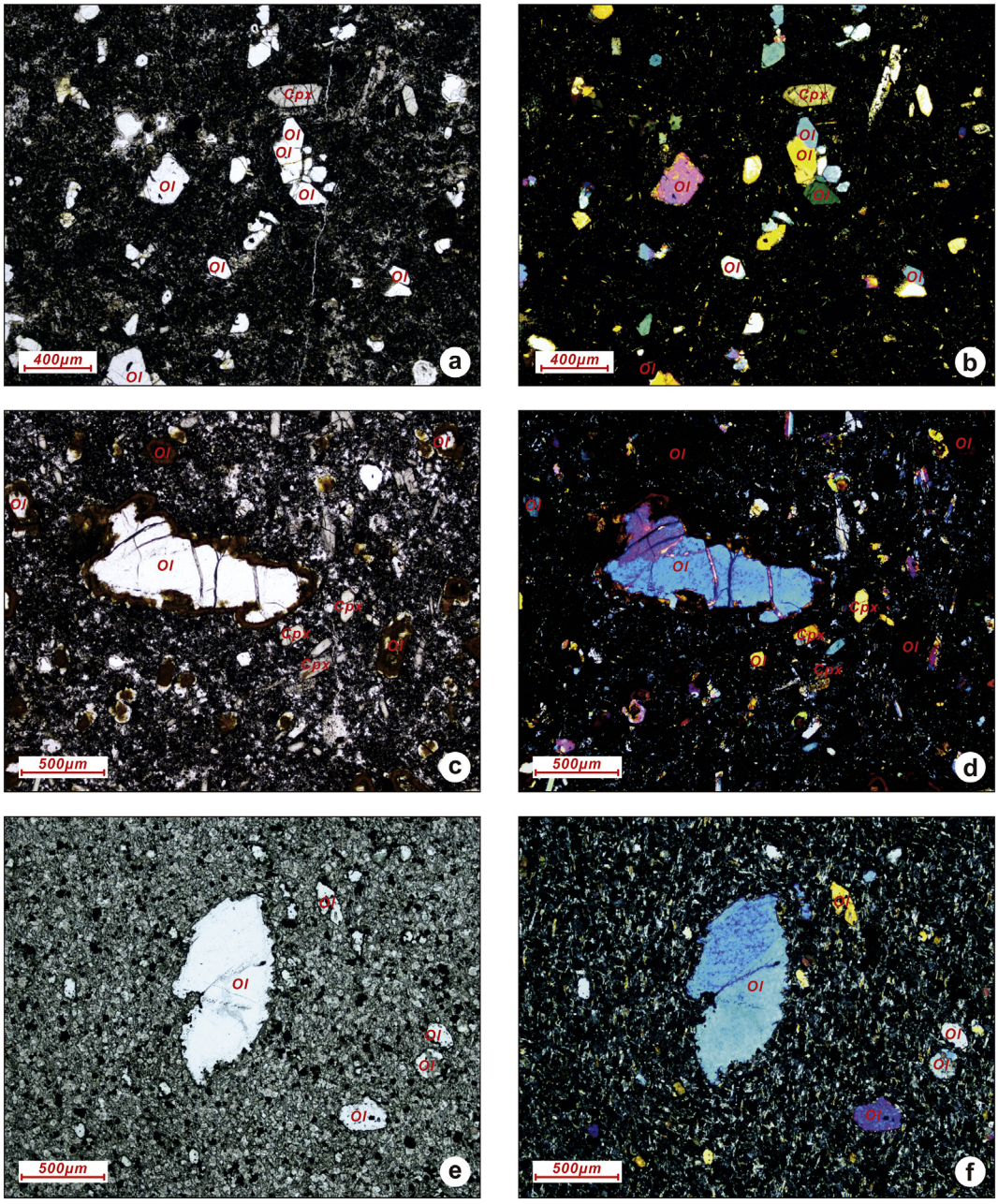

Fig. 3. Representative microphotographs of Jiaodong basalts: (a)–(b) weakly alkaline basalts, (c)–(f) strongly alkaline basalts. (a), (c) and (e) in transmission light, and others in crossed polarity. Mineral abbreviations: Ol for Olivine and Cpx for Clinopyroxene.

4. Results

Olivine compositions of the Jiaodong basalts are given in Table S5, with mean values summarized in Table 1. The analyzed olivine phenocrysts have low Fo values (79–84) and high CaO contents (>0.1 wt%), with 100Mn/Fe and Ni/(Mg/Fe)/1000 ratios of 1.1–2.0 and 0.4–1.0, respectively. Olivine 100Mn/Fe and Ni/(Mg/Fe)/1000 ratios respectively increase and decrease slightly with decreasing Fo values, consistent with the olivine fractionation trend (Fig. 4a, b). The strongly alkaline basalts generally have much higher 100Mn/Fe and lower Ni/(Mg/Fe)/1000 ratios than those of the weakly alkaline basalts (Fig. 4a, b) at fixed Fo values. These ratios plot in the field of olivines in peridotite- to pyroxenite-derived melts (Fig. 4c). Ni/(Mg/Fe)/1000 ratios of the olivines are strongly correlated with whole-rock compositions, including SiO_2 and $Fe_2O_3^T$ contents, and with Ba/Th, Ce/Pb, $^{87}Sr/^{86}Sr$, and $^{143}Nd/^{144}Nd$ ratios (Fig. 5).

The fO_2 values of the Jiaodong basalts were calculated using the $D_V^{olivine-melt}$ oxybarometer (Canil, 2002) following the empirical relationship:

$$D = a/\left(10^{(b\Delta NNO+c)} + 1\right) \quad (1)$$

where a = 0.9, b = 0.31, c = 1.53, and ΔNNO represents the logarithm deviation from the Ni–NiO oxygen buffer. fO_2 values are often expressed as the logarithm deviation from the FMQ buffer (ΔFMQ), and conversion from ΔNNO to ΔFMQ here involved the empirical relationship (Frost and McCammon, 2008):

$$\log fO_2 = A/T + B + C(P-1)/T \quad (2)$$

where A = −24,930 and −25,096.3, B = 9.36 and 8.735, and C = 0.046 and 0.110 for the NNO and FMQ buffers, respectively; and T and

Table 1
Summary of whole-rock and olivine compositions of the Jiaodong basalts, and calculated fO_2 values relative to the FMQ buffer.

		QX01	QX03	QX08	QX07	PL01	PL02	PL05	PL06	PL08	PL17	PL18
Whole rock[a]	SiO_2	41.52	41.34	41.51	42.15	47.12	46.76	44.71	46.2	49.1	40.19	40.37
	$Fe_2O_3^T$	15.33	15.26	15.39	15.40	12.93	12.93	13.49	13.97	12.51	16.25	16.31
	$Na_2O + K_2O$	6.4	7.13	7.21	6.74	5.9	6	6.28	6.87	5.05	8.38	7.99
	FeO/MnO	43.73	40.78	41.48	44.05	55.71	55.29	46.75	54.83	59.38	42.95	42.18
	CaO-CaO*	0.81	0.21	0.57	0.14	−2.39	−2.12	−1.11	−3.30	−2.38	−0.13	−0.11
	FC3MS	0.13	0.13	0.11	0.16	0.49	0.44	0.23	0.68	0.55	0.16	0.15
	$Fe^{3+}/\sum Fe$	0.30	0.32	0.31	0.30	0.19	0.19	0.23	0.21	0.16	0.35	0.37
	V	187	195	175	181	168	175	177	157	156	209	218
	Ba/Th	62	30	36	36	75	84	49	69	110	37	30
	Ce/Pb	35	35	32	30	26	27	28	23	26	103	123
	$^{87}Sr/^{86}Sr$	0.703778	0.703808	0.703695	0.703740	0.704233	0.704100	0.703955	0.704181	0.704338	0.703507	0.703496
	$^{143}Nd/^{144}Nd$	0.512866	0.512860	0.512878	0.512869	0.512785	0.512797	0.512851	0.512842	0.512785	0.512881	0.512880
Olivine[b]	Fo	81.29	80.89	80.56	80.33	80.84	81.41	82.54	79.76	82.11	81.55	81.55
	1σ	0.42	0.44	2.41	0.94	0.71	1.04	1.08	0.66	0.44	1.17	0.26
	100Mn/Fe	1.46	1.51	1.79	1.54	1.34	1.34	1.54	1.21	1.24	1.57	1.54
	1σ	0.12	0.22	0.52	0.15	0.02	0.03	0.09	0.01	0.02	0.21	0.11
	Ni/(Mg/Fe)	0.69	0.73	0.73	0.75	0.83	0.78	0.83	0.90	0.93	0.60	0.53
	1σ	0.10	0.10	0.24	0.06	0.05	0.04	0.07	0.03	0.08	0.13	0.06
	V	3.41	3.42	3.30	3.43	5.42	5.57	4.76	4.25	6.08	3.37	3.11
	1σ	0.58	0.73	0.72	0.83	0.29	0.30	0.50	0.24	0.28	0.64	0.59
Oxygen fugacity[c]	Dv	0.018	0.018	0.019	0.019	0.032	0.032	0.027	0.027	0.039	0.016	0.014
	1σ	0.003	0.004	0.004	0.005	0.002	0.002	0.003	0.002	0.002	0.003	0.003
	ΔFMQ	1.26	1.31	1.21	1.21	0.41	0.44	0.68	0.67	0.14	1.43	1.61
	1σ	0.24	0.29	0.33	0.36	0.08	0.08	0.15	0.08	0.07	0.29	0.26

[a] Whole-rock compositions of the Jiaodong basalts are volatile free; $Fe^{3+}/\Sigma Fe$ ratios were calculated using Petrolog software (Danyushevsky and Plechov, 2011) using the fO_2 values obtained in this study and the model of Kress and Carmichael (1988); CaO* = 13.81–0.274MgO (Herzberg and Asimow, 2008); FC3MS = (FeO/CaO) − 3(MgO/SiO_2) (Yang and Zhou, 2013); Only Fe^{2+} was considered in FeO/MnO and FC3MS.
[b] Olivine compositions are mean values.
[c] fO_2 values in the basalts were calculated using the model of Canil (2002) at a temperature of 1200 °C and a pressure of 1 atm.

P are in units of K and bar, respectively. The $D_V^{olivine-melt}$ oxybarometer (Canil, 2002) was chosen because it is widely applied in determining fO_2 values of natural magmas and yields fO_2 values virtually identical to those estimated by the Fe^{2+}/Fe^{3+} oxybarometer (e.g., fO_2 values of Siqueiros MORBs in Fig. 6; Kelley and Cottrell, 2012).

The Jiaodong basalts have V contents of 156–218 ppm, and olivines in the Jiaodong basalts have V contents in the range 3.11 ± 0.59 ppm to 6.08 ± 0.28 ppm (Table 1). $D_V^{olivine-melt}$ values of the Jiaodong basalts were obtained by simply assuming constant V contents in the melts during crystal fractionation. The calculated $D_V^{olivine-melt}$ values are 0.014 ± 0.003 to 0.039 ± 0.002 and ΔFMQ values of 1.61 ± 0.26 to 0.14 ± 0.07 (Table 1). The fO_2 values of the Jiaodong basalts are generally within the range of arc basalts, overlapping but slightly higher than OIB and MORB values (Fig. 6), and are correlated with whole-rock compositions (Fig. 7). Specifically, fO_2 values of the basalts are negatively correlated with SiO_2 contents and Ba/Th and $^{87}Sr/^{86}Sr$ ratios, and positively correlated with $Fe_2O_3^T$ contents and Ce/Pb and $^{143}Nd/^{144}Nd$ ratios (Fig. 7). The strongly alkaline basalts (ΔFMQ = 1.0–1.6) generally have much higher fO_2 values than the weakly alkaline basalts (ΔFMQ = 0.0–0.5).

5. Discussion

Our results indicate two main characteristics of the redox states of Jiaodong basalts: (a) high fO_2 values of up to ~ΔFMQ +1.6 (Fig. 6); and (b) a relatively wide fO_2 range (up to ~1.5 log units), with fO_2 values varying as a function of whole-rock compositions (Fig. 7). Any feasible model for the formation of oxidized domains in the convective mantle should account for these features, as discussed in the following sections.

5.1. Recycled-carbonate-induced mantle oxidation

The wide variations in Jiaodong basalt fO_2 values may be related with the assumption of constant V in the melts to obtain $D_V^{olivine-melt}$ and fO_2 values. This assumption was primarily built on the fact of the <10% olivine fractionation (clinopyroxene ignored due to its minor amount) to form the narrow Fo variations of olivines in each samples (ΔFo usually <3; Table S5; Fig. S1). Olivine usually have $D_V^{olivine-melt}$ values of 0.01–0.1 in natural magmas with normal redox state (ΔFMQ = −1–2; Mallmann and O'Neill, 2009); <10% fractionation would increase V < 10% in the residual melts and uncertainty in ΔFMQ values <0.15 log units (Fig. S1a). As shown in Fig. S1b, many basalts (primarily the strongly alkaline basalts) and their olivine phenocrysts are in disequilibrium, due to bearing olivine xenocrysts (≤6%; Table S1). Subtracting these olivine xenocrysts in the basalts would produce the uncertainty in ΔFMQ values <0.1 log units (Fig. S1a). Therefore, assumption of constant V in the melts to obtain $D_V^{olivine-melt}$ values would cause the total uncertainty in ΔFMQ values <0.25 log units, which are extremely small when comparing with the large ΔFMQ variations of the basalts (up to ~1.5 log units).

The wide fO_2 variations in Jiaodong basalt may be due to magmatic processes, including crustal contamination, crystal fractionation and degassing (e.g., Kelley and Cottrell, 2012; De Moor et al., 2013; Brounce et al., 2014, 2017; Humphreys et al., 2015; Moussallam et al., 2014, 2016; Nicklas et al., 2019). The Jiaodong basalts have positive Nb—Ta anomalies and negative Pb anomalies in their primitive-mantle-normalized spider diagrams (Fig. 2f; Zeng et al., 2010; Sakuyama et al., 2013), and high Ce/Pb ratios of 22–120 (Fig. 2d). These characteristics are the converse of those of crustal components, which have negative Nb—Ta anomalies, positive Pb anomalies, and low Ce/Pb ratios of <10 (Rudnick and Gao, 2003), suggesting insignificant crustal contamination. Furthermore, crystal fractionation usually results in moderate oxidation of the melts (<0.5 ΔFMQ log units; e.g., Cottrell and Kelley, 2011; Brounce et al., 2014), much less than the observed fO_2 variations in the Jiaodong basalts (up to ~1.5 log units; Fig. 6). For example, there is lack of systematic differences in fO_2 values in MORBs with MgO > 8.5 wt%, MgO = 8.5–8.0 wt%, MgO = 8.0–7.0 wt%, and MgO = 7.0–6.0 wt%, suggesting that crystal fractionation has little effect on fO_2 in the basalts (Fig. 6). More importantly, crystal fractionation cannot change Ce/Pb or Ba/Th ratios or Sr—Nd isotopic compositions and therefore fails to explain the observed fO_2–composition correlations of the basalts (Fig. 7). Magma degassing is an

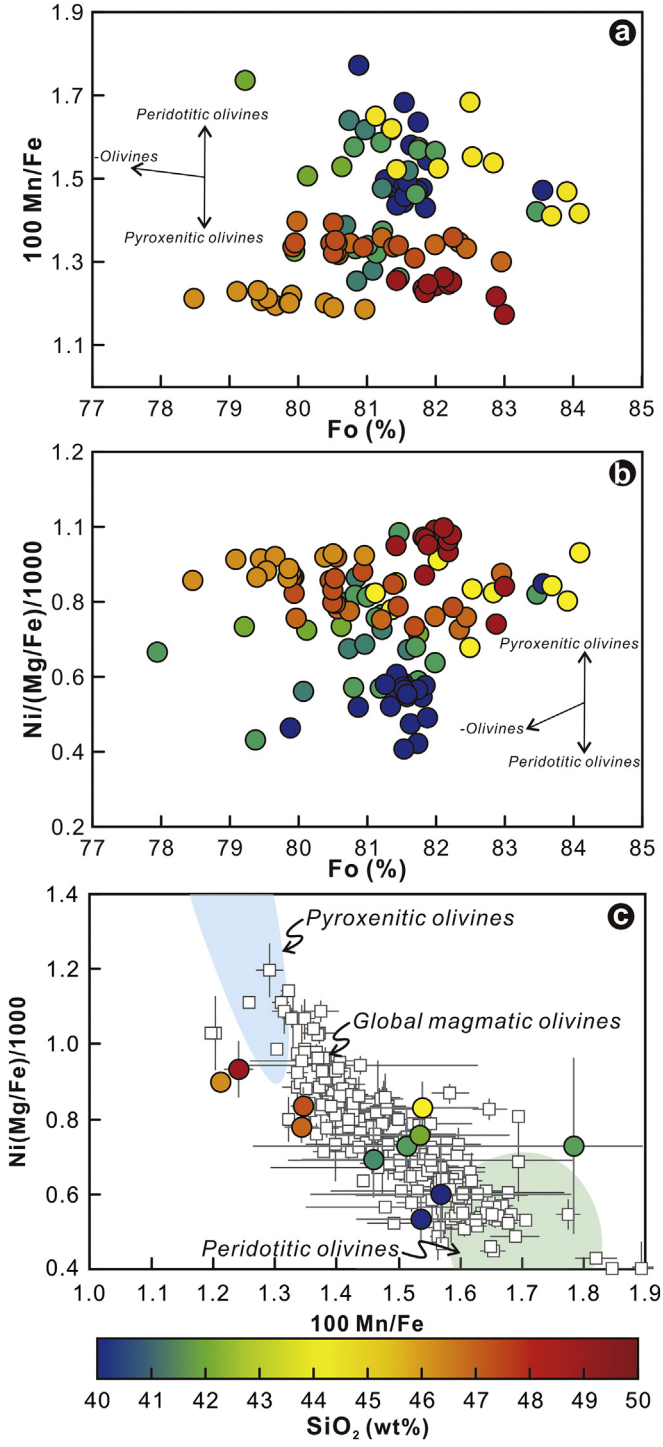

Fig. 4. Plots of olivine compositions of Jiaodong basalts: (a) (100Mn/Fe)–Fo; (b) (Ni/(Mg/Fe)/1000)–Fo; (c) mean (Ni/(Mg/Fe)/1000)–(100 Mn/Fe). The colour bar indicates the relative SiO_2 content of each sample. The global average compositions of magmatic olivines were from http://georoc.mpch-mainz.gwdg.de/georoc/.

effective way to alter redox state of magmas (e.g., Kelley and Cottrell, 2012; De Moor et al., 2013; Brounce et al., 2014, 2017; Moussallam et al., 2014, 2016; Humphreys et al., 2015). In all the gas components, degassing of sulfur has been demonstrated to have a critical control on the fO_2 values of evolving magmas (Moussallam et al., 2014, 2016; Brounce et al., 2017). Sulfur is primarily present as S^{2-} in mantle-derived magmas and is degassed primarily as SO_2 near the Earth surface; degassing of sulfur would substantially decrease fO_2 values of the melts (e.g., Moussallam et al., 2014, 2016; Brounce et al., 2017). During magma evolution, degassing of sulfur may happen before olivine crystallization. In this scheme, the method of using $D_V^{olivine-melt}$ to determine fO_2 of melts would fail to constrain the redox state of the melts before degassing; the results can only represent the redox state of the instantaneous evolved melts at the time of the olivine formation. Although presently we cannot exclude the possibility of sulfur degassing before olivine formation, due to poor constrain on sulfur contents in the Jiaodong basalts, we suggest that this possibility seems impossibly, given the reasons below. (1) Degassing of sulfur usually happens near the Earth surface (e.g., Brounce et al., 2017), whereas olivine usually crystallizes at much deeper depth, implying that olivine forms before degassing of sulfur. (2) Degassing of sulfur would substantially decrease fO_2 values of the melts (e.g., Moussallam et al., 2014, 2016; Brounce et al., 2017), but many Jiaodong basalts still have high fO_2 values (ΔFMQ >0.5) and each samples have relatively homogeneous ΔFMQ values (1 sigma <0.4 log units). (3) Degassing of sulfur cannot change basalt compositions including SiO_2, Fe_2O_3, Ba/Th, Ce/Pb and Sr—Nd isotopes, thus, cannot explain the observed fO_2–composition relationships of the Jiaodong basalts.

Melting temperature and pressure may influence fO_2 in the mantle when deduced from the fO_2 values of the magmas at 1 atm. At constant pressure, an increase in temperature can lead to a decrease in the fO_2 of silicate liquid, but the change in ΔFMQ is negligible (<0.1 log units from 1200 to 1700 °C; Kress and Carmichael, 1991; Brounce et al., 2017). On the other hand, the effect of pressure on ΔFMQ is not negligible. For solid silicate materials, increasing pressure would decrease fO_2 values in the mantle (~ 0.7 log units per GPa relative to the FMQ buffer; Foley, 2011; Frost and McCammon, 2008). In contrast, the ΔFMQ of silicate liquid increases slightly with increasing pressure at a rate of ~0.17 log units per GPa (Kress and Carmichael, 1991). In the Jiaodong region, the strongly alkaline basalts have low SiO_2, high $Fe_2O_3^T$ and negative Zr–Hf–Ti anomalies (Zeng et al., 2010; Sakuyama et al., 2013; Fig. 2), similar to experimental melts of carbonate-bearing mantle rocks (Dasgupta et al., 2006, 2009), whereas the weakly alkaline basalts have much higher SiO_2, lower $Fe_2O_3^T$ and no Zr-Hf-Ti anomalies. These different geochemical features suggest that the strongly and weakly alkaline basalts are derived from the CO_2 -rich and -poor mantle source, respectively (Zeng et al., 2010; Sakuyama et al., 2013; Li et al., 2016; Zhang et al., 2017). Furthermore, experiments have demonstrated that carbonate-induced depression of mantle rock solidus (Dasgupta and Hirschmann, 2010) would cause carbonate-bearing rocks to start melting at a much greater depth (>150 km; Dasgupta and Hirschmann, 2010; Rohrbach and Schmidt, 2011; Dasgupta et al., 2013) compared with carbonate-free rocks (~100 km; Spandler et al., 2008). This suggests that the strongly alkaline basalts are derived from a deeper mantle source than the weakly alkaline basalts, elevating more ΔFMQ values in the mantle source while considering the positive effect of pressure on the fO_2 of silicate melt. Because the strongly alkaline basalts tend to have higher ΔFMQ values than the weakly alkaline basalts (Fig. 7), their mantle source would still be more oxidizing than that of the latter. The mantle source of the strongly alkaline basalts corrected to the depth of the shallower mantle source of the weakly alkaline basalts, if not melt, would increase ΔFMQ values, exhibiting more oxidizing feature than the latter, too. More importantly, because the geochemical compositions (Ce/Pb, Ba/Th and Sr—Nd isotopes) of the basalts are usually independent with the melting pressure, different melting pressure in the mantle cannot explain the observed fO_2–composition relationships in the Jiaodong basalts, too.

We therefore conclude that fO_2 variations in the Jiaodong basalts reflect primarily the heterogeneity of oxidation states in the mantle source, with their fO_2–composition trends indicating two distinctive mantle redox domains, namely, oxidized and reduced domains for strongly and weakly alkaline basalts, respectively. The derivation of strongly alkaline basalts from an oxidized mantle source is supported by other observations, as follows. The strongly alkaline basalts with

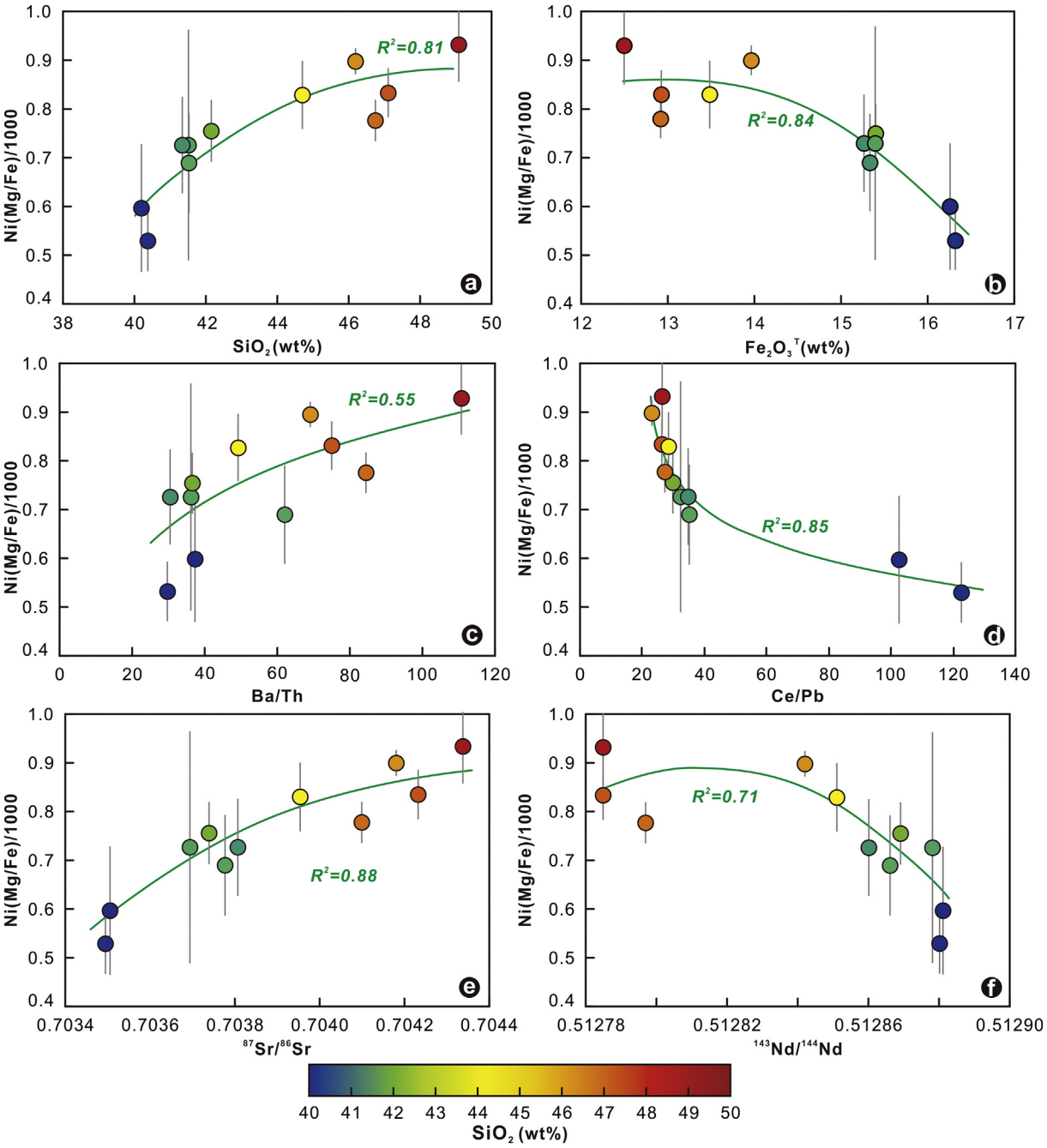

Fig. 5. Plots of Ni/(Mg/Fe)/1000$_{olivine}$ versus whole-rock compositions of the Jiaodong basalts for (a) SiO_2; (b) $Fe_2O_3^T$; (c) Ba/Th; (d) Ce/Pb; (e) $^{87}Sr/^{86}Sr$; (f) $^{143}Nd/^{144}Nd$.

low SiO_2, high $Fe_2O_3^T$ and negative Zr-Hf-Ti anomalies (Fig. 2) suggest the carbonate-bearing mantle source formed under highly oxidized conditions (Dasgupta et al., 2006, 2009). Their high $\delta^{56}Fe$ values (up to 0.29‰) also require a source oxidation state sufficient to fractionate Fe isotopes (He et al., 2019). Nevertheless, whether recycled carbonate (Rohrbach and Schmidt, 2011; Sun and Dasgupta, 2019; Thomson et al., 2016) or recycled oceanic crust (Brounce et al., 2017; Shorttle et al., 2015) caused the mantle oxidization remains a subject of debate.

The OIB-like compositions of the Jiaodong basalts suggest a recycled oceanic crust component in the source (Zhang et al., 2009; Xu et al., 2012; Sakuyama et al., 2013; Xu, 2014; Li et al., 2016). Owing to its much lower solidus, recycled oceanic crust (in the form of eclogite) melts before peridotite, producing SiO_2-rich melts followed by pyroxenite via reaction with ambient peridotite (Herzberg, 2011; Sobolev et al., 2005). The relative contributions of pyroxenite and peridotite to basalt genesis depend on the extent of partial melting and can be assessed by the compositions of olivine phenocrysts (Sobolev et al., 2005; Herzberg, 2011; Fig. 4c). Because pyroxenite has much lower D_{Ni} and higher $D_{Mn/Fe}$ (D_{Ni} and $D_{Mn/Fe}$ are Ni and Mn/Fe partition coefficients) values than peridotite, melts from pyroxenite would crystallize olivines with higher Ni/(Mg/Fe)/1000 and lower 100Mn/Fe ratios (Herzberg, 2011; Sobolev et al., 2005). The strongly alkaline Jiaodong basalts generally have higher 100Mn/Fe and lower Ni/(Mg/Fe)/1000 ratios than the weakly alkaline basalts (Fig. 4). All the analytical olivine phenocrysts in the Jiaodong basalts have relatively low Fo values (Fo < 85), possibly suggesting some extend of crystal fractionation in the early stages. Nonetheless, these basalts primarily underwent olivine-controlled fractionation, which has subtle influence on

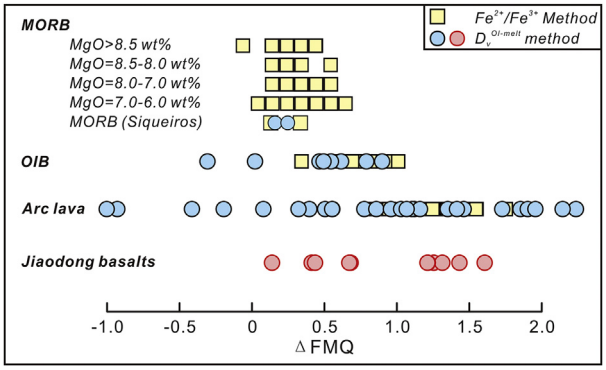

Fig. 6. Comparisons of fO_2 values relative to FMQ (ΔFMQ) between the Jiaodong basalts and other basaltic lavas. Fe^{2+}/Fe^{3+} ratios of the lavas and olivine and whole-rock compositions are from http://georoc.mpch-mainz.gwdg.de/georoc/ and http://www.earthchem.org/petdb/search. Only the Fe^{2+}/Fe^{3+} data measured by micro X-ray absorption near-edge structure (μ-XANES) spectroscopy were considered here.

Ni/(Mg/Fe)/1000 and 100 Mn/Fe of olivines (Sobolev et al., 2007; Herzberg, 2011; Figs. 4a, b). Therefore, the Ni/(Mg/Fe)/1000 and 100 Mn/Fe ratios of the low Fo olivines can still record the features of the olivines in the primitive melts. Olivine Ni/(Mg/Fe)/1000 ratios of the Jiaodong basalts are correlated with their whole-rock compositions (Ba/Th, Ce/Pb, $^{87}Sr/^{86}Sr$, and $^{143}Nd/^{144}Nd$ ratios; Figs. 5c–f), which are unrelated to magmatic processes, further indicating primary control of olivine compositions by source lithology, with peridotite-derived and pyroxenite-derived melts for strongly and weakly alkaline basalts, respectively. Furthermore, peridotitic melts typically have lower FeO/MnO and FC3MS values [FC3MS = (FeO/CaO) − 3(MgO/SiO_2); Yang and Zhou, 2013)], higher CaO − CaO* (CaO* = 13.81–0.274MgO) ratios (Herzberg and Asimow, 2008), compared with pyroxenitic melts. We only used Fe^{2+}, not Fe^{total}, to calculate FeO/MnO and FC3MS values, because in the highly oxidizing melts such as the strongly alkaline basalts, increase of Fe^{3+} would significantly elevate FeO/MnO and FC3MS. The strongly alkaline basalts have lower FeO/MnO and FC3MS and higher CaO − CaO* values than the weakly alkaline basalts (Fig. 8), further

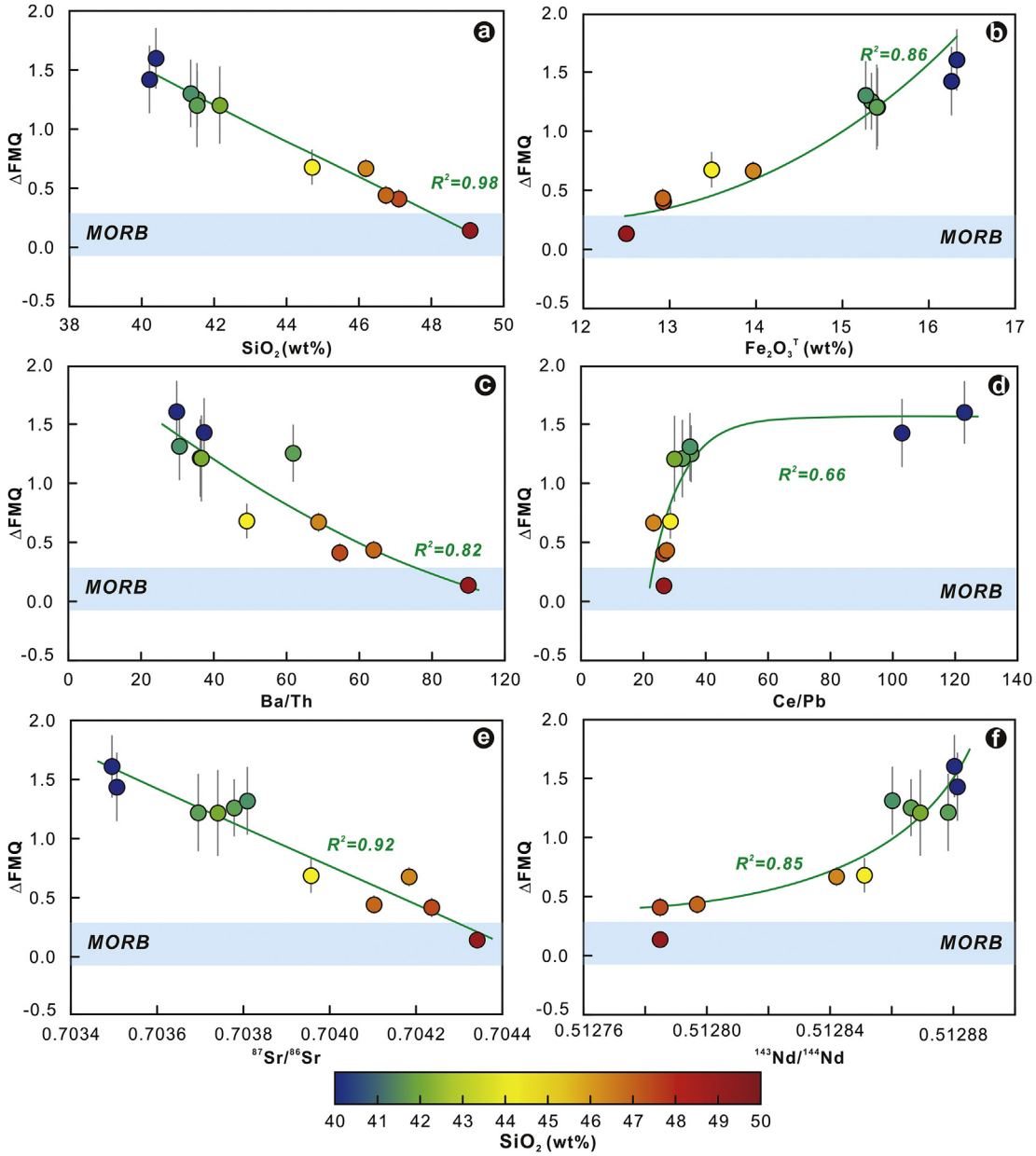

Fig. 7. ΔFMQ versus whole-rock compositions of the Jiaodong basalts for (a) SiO_2; (b) $Fe_2O_3^T$; (c) Ba/Th; (d) Ce/Pb; (e) $^{87}Sr/^{86}Sr$; and (f) and $^{143}Nd/^{144}Nd$. The blue shaded area marks the ΔFMQ of MORB (0.10 ± 0.18; Cottrell and Kelley, 2011).

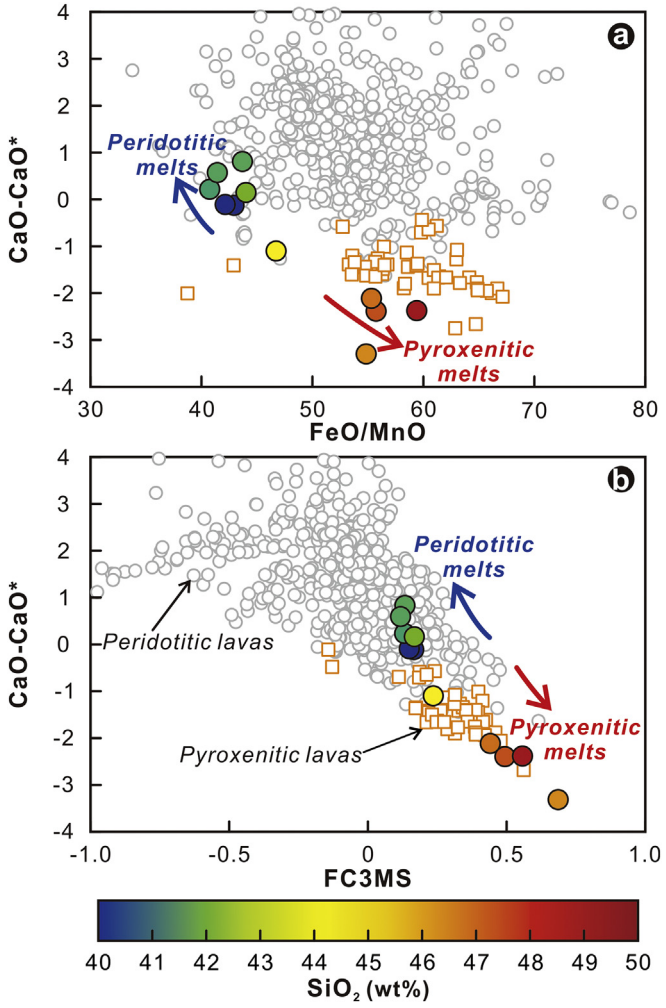

Fig. 8. Discrimination plots for mantle source lithologies of the Jiaodong basalts: (a) (CaO − CaO*)–(FeO/MnO); (b) (CaO − CaO*)–FC3MS. FC3MS = (FeO/CaO) − 3 (MgO/SiO_2) (Yang and Zhou, 2013); CaO* = 13.81–0.274MgO; the boundary line between peridotitic and pyroxenitic melts was defined by Herzberg and Asimow (2008). All the data are from http://georoc.mpch-mainz.gwdg.de/georoc/ with the exception of MORBs (http://www.earthchem.org/petdb/search).

supporting higher proportions of peridotite-derived melts in the former. The fO_2 values of the Jiaodong basalts are correlated with whole-rock source lithological indices (FeO/MnO, FC3MS, and CaO − CaO*) and olivine Ni/(Mg/Fe)/1000 values, and decrease with increasing reduction of pyroxenite-derived melts (Fig. 9). These observations suggest that the source with more pyroxenite is more reduced and that recycled oceanic crust did not oxidize the mantle. This conclusion is apparently inconsistent with the oxidation state of oceanic crust on the seafloor, but it may be understood if a redox transformation occurs in the subducting slab through the release of oxidative fluids and melts to the mantle wedge during subduction. The gradual decrease in fO_2 from arc- to backarc-related lavas (Brounce et al., 2014; Kelley and Cottrell, 2009, 2012) is consistent with the decreasing ingress of fluids from the subducting slab to the overlying mantle wedge, with the slab thus becoming less oxidized during subduction. This conclusion is supported by the comparable reduction state between mantle peridotite and eclogite, vestiges of subducted oceanic crust (Stagno et al., 2015), and enriched mantle containing more recycled crustal components being more reduced than the ambient mantle (Cottrell and Kelley, 2013).

Like Sr—Nd isotopes, δ^{26}Mg and δ^{66}Zn of the basalts do not fractionate significantly during magma processes, thus, can record the features of the mantle source. The abnormally low δ^{26}Mg and high δ^{66}Zn values of the Jiaodong basalts (He et al., 2019; Wang et al., 2018) signify recycled carbonates in their mantle source (Fig. S2), as carbonate is the only known natural material with low δ^{26}Mg and high δ^{66}Zn values (Li et al., 2017; Liu et al., 2016). δ^{66}Zn values, together with fO_2 variability, gradually increase from the weakly to strongly alkaline basalts (Figs. S2 and 7). These observations further indicate the involvement of recycled carbonate as a mantle oxidant.

There are three different carbonate reservoirs in the oceanic lithosphere, namely, sediment, altered oceanic crust, and sub-lithospheric mantle (e.g., Kelemenn and Mann, 2015). The OIB-like trace-element and depleted Sr—Nd isotopic compositions of the Jiaodong basalts indicate that the recycled carbonate is derived primarily from igneous oceanic crust (Sakuyama et al., 2013). It has been experimentally shown that carbonate-bearing igneous oceanic crust melts when the subducted slab reaches the mantle transition zone (Thomson et al., 2016). There is little evidence for recycled carbonate sediment in the Jiaodong basalts, suggesting that it had been detached from the subducted slab before entering the mantle transition zone, possibly on account of its positive buoyancy in the ambient mantle (Dasgupta, 2013). Carbonate-bearing oceanic sub-lithospheric mantle apparently does not melt in the mantle transition zone because of its much higher solidus (Fig. 10). We propose a two-stage model for the formation of oxidized domains in the convective mantle (Fig. 10), as follows.

Stage 1: Melting of carbonate-bearing slab. As the subducted slab delivered carbonate-bearing igneous oceanic crust to the deep mantle, a steep solidus depression would trigger melting of this crust, producing strongly oxidized carbonate-rich melts with high Fe_2O_3, Al_2O_3, and CaO contents (Thomson et al., 2016).

Stage 2: Redox 'freezing'. Owing to their ultra-low viscosity (Kono et al., 2014), the carbonate-rich melts would flow out of the slab and infiltrate the reduced ambient mantle (Rohrbach and Schmidt, 2011). Under such reducing conditions, the melts would be unstable and reduced to diamond (Thomson et al., 2016). Expulsion of the oxidizing and fertile carbonate-rich melts from the slab would also cause the oxidation and re-fertilization of ambient mantle (Rohrbach and Schmidt, 2011; Thomson et al., 2016), whereas the reduction of carbonate to carbon would produce oxidized domains in the deep mantle. It is possible that abundant recycled carbonate may be in excess to redox freezing and possibly lead to carbonate-fluxed peridotite melting, but considering too much reduced materials in convective mantle when comparing with abundance of the recycled carbonate-rich melts, the carbonate-rich melts are more likely reduced to carbon completely. The link between fO_2 values of the oceanic basalts and their compositions (Cottrell and Kelley, 2013; Shorttle et al., 2015) indicates that recycled components may be stored in the convective mantle for billions of years (Hofmann, 1997; White, 2010), with redox-state heterogeneity being preserved in the convective mantle over tectonic timescales (Cottrell and Kelley, 2013).

5.2. fO_2 variability due to differential melting within a heterogeneous mantle

As discussed in Section 5.1, the oxidizing strongly alkaline basalts were derived from a deep carbonate-bearing peridotite source, whereas the reduced weakly alkaline basalts were partial melts of carbonate-free pyroxenite in much shallower depth. This implies an inverse depth–fO_2 profile in the convective mantle, with oxidation increasing with depth. A more oxidized convective mantle at greater depth is also indicated by other studies of natural lavas beyond convergent regions. OIBs usually form in the convective mantle at greater depths than do MORBs, and tend to have much higher fO_2 values relative to MORBs (Shorttle et al., 2015; Brounce et al., 2017; Fig. 6). The inferred inverse depth–fO_2 profile in the convective mantle is inconsistent with the general recognition that the redox state of the convective mantle becomes

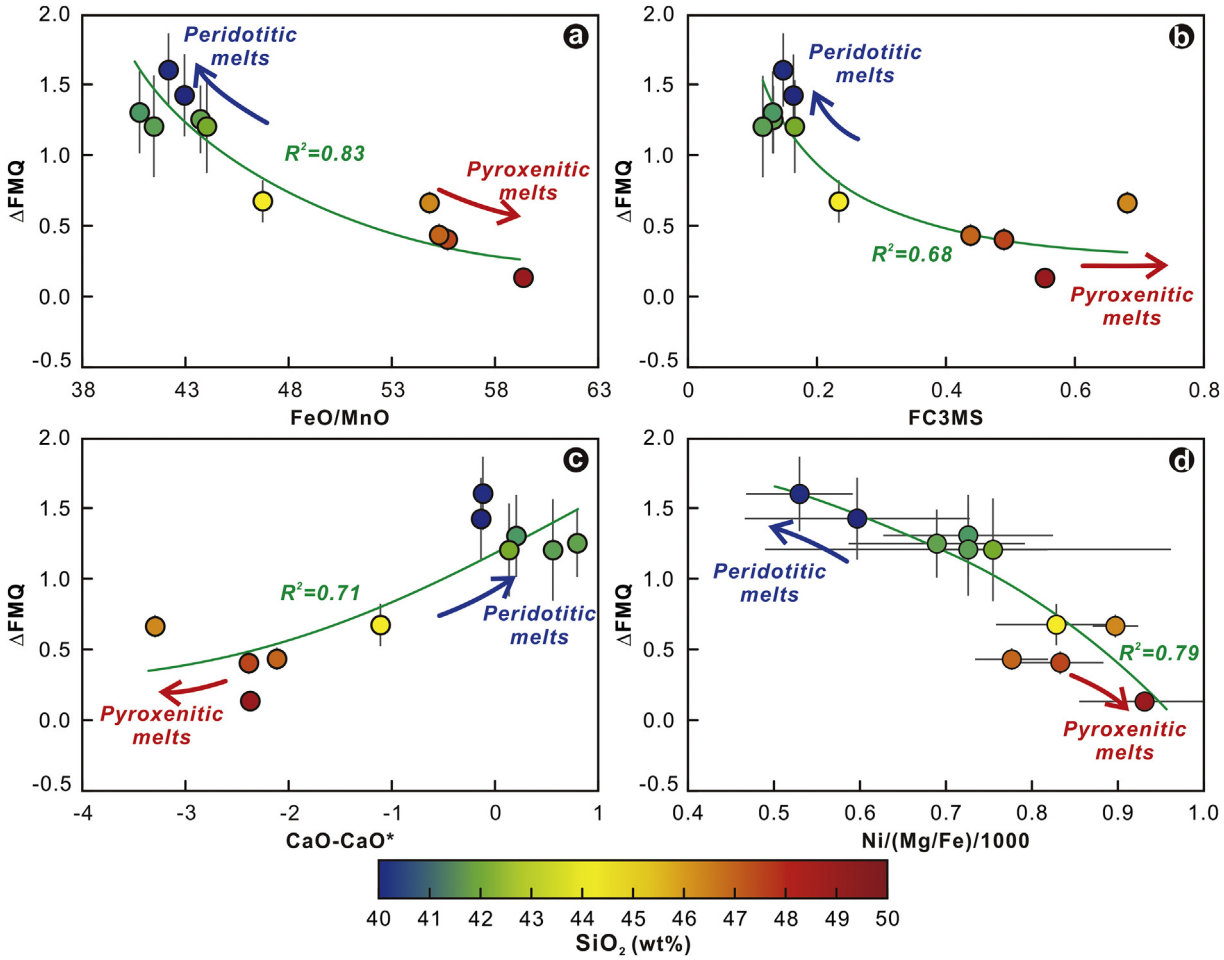

Fig. 9. ΔFMQ versus various geochemical signals of source lithologies in the Jiaodong basalts: (a) FeO/MnO, (b) FC3MS, and (c) CaO − CaO* whole-rock values; and (d) Ni/(Mg/Fe)/1000 values of olivines.

increasingly reduced as depth increases (Eguchi and Dasgupta, 2018; Frost and McCammon, 2008).

Whether or not there is an inverse depth–fO_2 profile depends strongly on the assumption that the redox state of the mantle basalt source is fully equilibrated with that of ambient mantle. It is known that heterogeneous components occur in the convective mantle (Herzberg, 2011; Hofmann, 1997; Sobolev et al., 2005; White, 2010). Furthermore, the end-member basalts have different fO_2 values (Cottrell and Kelley, 2013; Shorttle et al., 2015; this study), suggesting a heterogeneous redox state in the convective mantle and thus a lack of equilibrium between the mantle basalt source and ambient mantle. Basalt fO_2 values may therefore reflect only the redox state of related components in the mantle source, rather than those of large-scale mantle domains. In that case, the observed variability of fO_2 values in Jiaodong basalts most likely resulted from differential melting of a heterogeneous mantle. The strongly and weakly alkaline basalts would have been formed in the same upwelling mantle column but at different mantle depths, with the strongly alkaline basalts (with higher fO_2 values) originating from oxidized carbonate-bearing peridotite at deeper depths, and the weakly alkaline basalts from reduced pyroxenite at much shallower depths (Fig. 10). We propose a two-stage model for the formation of the Jiaodong basalts (Fig. 10), as follows.

(1) Mantle upwelling, probably induced by rollback of the subducting Pacific slab (Xu et al., 2018), carried diamond-bearing peridotite that had been oxidized by carbonate-rich melts from the subducted slab (Section 5.1) and carbonate-free eclogitic fragments detached from the stagnant slab. This upwelling process would further elevate fO_2 values in the mantle as a result of the increasing instability of the Fe^{3+}-bearing skiagite component of garnet at shallower depths (Gudmundsson and Wood, 1995). When the oxidation state was sufficiently high, diamond in the oxidized domain would have been re-oxidized to carbonate (Rohrbach and Schmidt, 2011). The reappearance of carbonate would have triggered peridotite melting to first form carbonatitic melts and then strongly alkaline basalts at shallower depths (Dasgupta et al., 2013). Because the redox partial melting is self-driven reaction, the redox state of the local mantle during the reaction is invariable, and the partial melts would also preserve the oxidized state of the mantle. The redox melting reaction of oxidized peridotite would probably have occurred at depths of ~300 km, slightly deeper than normal mantle (150–250 km; e.g., Dasgupta et al., 2013; Rohrbach and Schmidt, 2011; Stagno et al., 2013).

(2) Carbonate-free eclogitic fragments have a slightly higher solidus than carbonated peridotites and would melt after carbonate-bearing peridotite at a shallower depth (~120 km; Takahashi et al., 1998). Their SiO_2-rich partial melts would react with peridotite to form pyroxenite, which would melt at depths of ~100 km (Spandler et al., 2008), leading to the formation of weakly alkaline basalts. The volatile-free ambient peridotite has the higher solidus and would melt just below the Jiaodong region where the lithosphere is ~80 km thick.

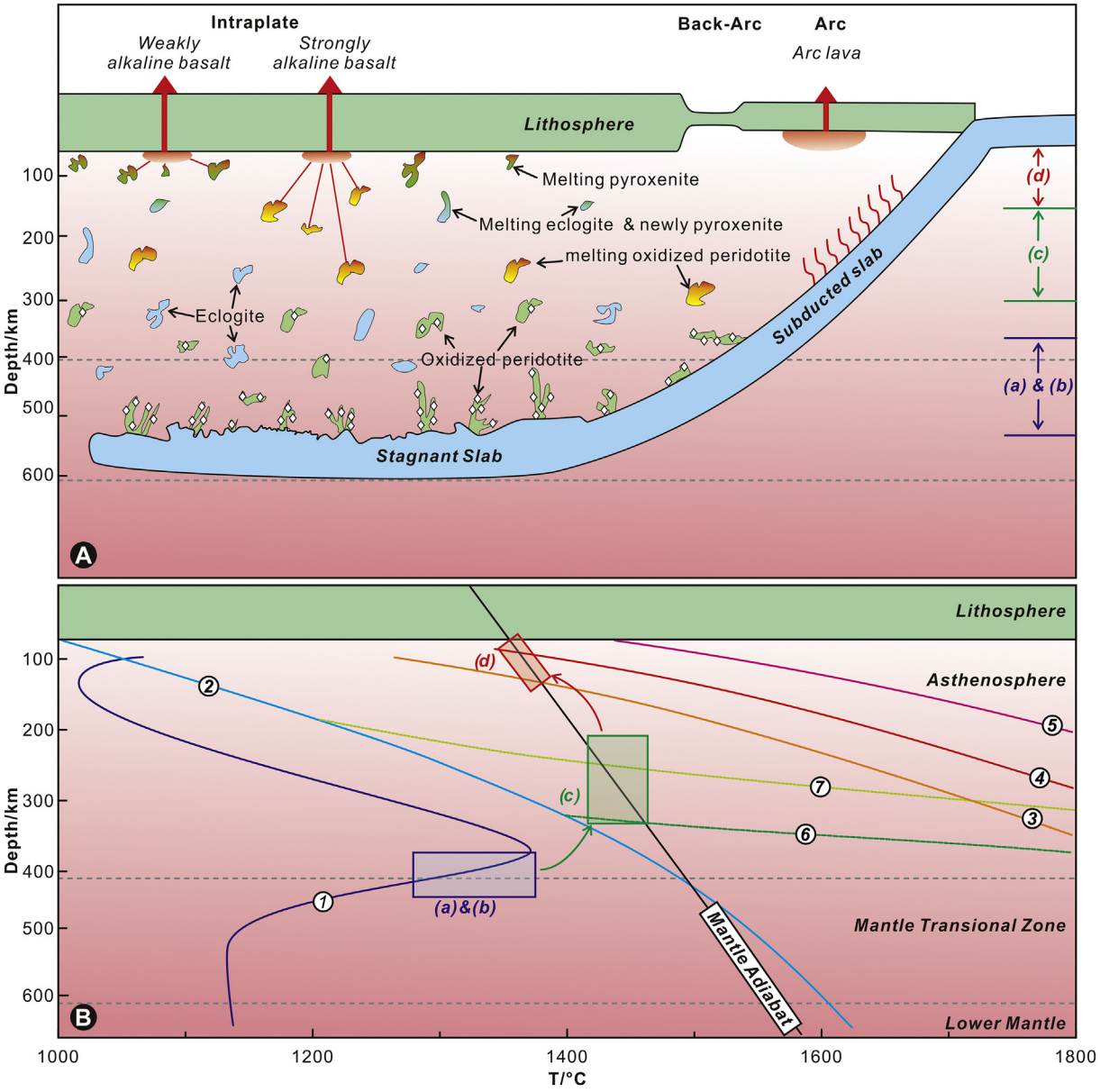

Fig. 10. (A) Conceptual model for mantle oxidation and formation of the Cenozoic Jiaodong basalts. (a) Subduction delivers carbonate to the deep mantle, which drives slab melting to generate carbonate-rich melts; (b) redox freezing occurs through reaction of carbonate-rich melts with highly reduced ambient mantle, resulting in diamond formation and mantle oxidation; (c) with mantle upwelling, diamond-bearing mantle in the oxidized domain first drives redox melting at ~300 km depth, with diamond being replaced by carbonate, forming strongly alkaline basalts; (d) further mantle upwelling causes melting of carbonate-free eclogite, forming SiO_2-rich melts and subsequently pyroxenite, with melts formed at shallower depths forming weakly alkaline basalts. (B) Solidus of various rocks under mantle conditions: 1 carbonated eclogite, 2 carbonated peridotite, 3 eclogite, 4 pyroxenite, 5 peridotite, 6 and 7 redox melting of mantle peridotite beneath eastern China and on a global scale, respectively. A mantle adiabat with a potential temperature of 1315 °C is assumed (McKenzie et al., 2005). The solidus lines (1, 2, 3, 5, and 7) are from Dasgupta et al. (2004), Dasgupta and Hirschmann (2010) Dsgupta and Hirshcmann, 2010, Thomson et al. (2016), Hirschmann (2000) Hirschamnn, 2000, and Takahashi et al. (1998) Takahashi et al., 1998. High fO_2 values in the deep mantle (due to cycling of carbonate) beneath eastern China trigger redox melting at slightly greater depths (~300 km) than in other regions (~200 km).

This interpretation does not preclude the possibility of an oxidized lowermost upper mantle, as mantle oxidation usually takes place at the bottom of the upper mantle within the transition zone because of the continuous interaction between the stagnant slab and the overlying mantle wedge (Li et al., 2017; Xu et al., 2018).

5.3. Implications

The recycled-carbonate-induced mantle oxidation model yields some insights into the geodynamic processes that occur in the deep mantle.

Geophysical studies have detected global low seismic velocity anomalies and high electrical conductivities in the asthenosphere, usually extending to a depth of ~200 km (e.g., Gu et al., 2005; Lizarralde et al., 1995), close to the mantle depth where the redox melting reaction begins to occur (Rohrbach and Schmidt, 2011; Stagno et al., 2013; Dasgupta et al., 2013). Redox melting produces carbonatite-rich melts, effectively increasing electrical conductivity and decreasing seismic velocity (Gaillard et al., 2008; Sifré et al., 2014), so these geophysical anomalies are commonly attributable to the presence of carbonatite-rich melts in the deep mantle. However, beneath eastern China, the anomalies extend to much greater depths (>300 km; Karato, 2010; Huang and Zhao, 2006), where the mantle is usually assumed to be

highly reduced and metal saturated, with unstable carbonates (Rohrbach and Schmidt, 2011). However, carbonate stability at such depths may be achieved if the mantle there has been oxidized (Rohrbach and Schmidt, 2011). This may occur through two stages: (1) incorporation of carbonate-rich melts from the stagnant subducted Pacific slab into the mantle transition zone to oxidize the ambient mantle with reduction of carbonate to diamond; and (2) re-oxidation of diamond to carbonate during upwelling. The unusual vertical extent of the seismic velocity and electrical conductivity anomalies in eastern China would then be consistent with results of petrological and isotopic studies (Li et al., 2017; Liu et al., 2016; Wang et al., 2018).

Recent studies have revealed a gradual increase in fO_2 values in the mantle during the period 3.5–1.8 Ga (with ΔFMQ up to ~1.3 log units; Aulbach and Stagno, 2016; Nicklas et al., 2019). Mantle oxidization across the Archean–Proterozoic boundary is coupled with the Great Oxidation Event of ca. 2.4–2.3 Ga (Bekker and Holland, 2012), suggesting an intimate link with the oxidation state of the atmosphere. Several models including recycled oceanic crust and mixing of highly oxidized lower mantle with incorporation of metallic Fe into the core have been proposed to explain this secular mantle oxidation (Frost and McCammon, 2008; Nicklas et al., 2019). Precambrian sedimentary records indicate that Archean carbonate rocks became more abundant from ca. 3.5 Ga (Shaw, 2008), whereas fossil subduction markers such as the geochemical 'arc' signatures in various igneous rocks, structural thrust belts and dipping seismic reflectors, and high-pressure/low-temperature and low-pressure/high-temperature paired metamorphic belts, indicate that subduction had probably begun at ca. 3.2 Ga (van Hunen and Moyen, 2012Van Hunen and Moyen, 2012). The cycling of carbonates may therefore have begun as early as ca. 3.2 Ga. From the perspective of this study, episodic cycling of carbonate via subduction would probably have shaped mantle oxidation across the Archean–Proterozoic transition.

6. Conclusion

The application of V olivine–whole-rock distribution coefficients in determining redox states of Cenozoic Jiaodong basalts in eastern China reveals high and highly variable fO_2 values of 1.61 ± 0.26 to 0.14 ± 0.07 log units above the FMQ buffer. The fO_2 variations are correlated with whole-rock compositions, suggesting that they reflect their mantle source. Recycled carbonate within the oceanic crust oxidizes the mantle, rather than recycled oceanic crust. We suggest that the fO_2 values of the basalts reflect only the redox state of the relevant components in the mantle source. Oxidizing strongly alkaline basalts are from much greater depths in the convection mantle compared with the reduced weakly alkaline basalts because of differential melting in an upwelling heterogeneous mantle. Results of this study provide insights into the evolution of the redox state of the convective mantle.

Declaration of Competing Interest

The authors declare that they have no known competing financial interests or personal relationships that could have appeared to influence the work reported in this paper.

Acknowledgements

We gratefully acknowledge reviews by two anonymous referees, as well as editorial handling by Xianhua Li. We thank Chen L.L. for technical assistance with EPMA analysis, and staff at the Wuhan Sample Solution Analytical Technology Co. for technical assistance with bulk rock analyses. We gratefully acknowledge the financial support from Strategic Priority Research Program (B) of Chinese Academy of Sciences (Grant No. XDB18000000), the National Program on Global Change and Air-Sea Interaction (GASI-GEOGE-02) and the NSFC (41688103) to Y.G. X., the NSFC (41403024) and the State Key Laboratory of Isotope Geochemistry, GIG-CAS (SKLaBIG-QD-16-05) to L.-B. H. This is contribution No.IS-2847 from GIG-CAS.

Appendix A. Supplementary data

Supplementary data to this article can be found online at https://doi.org/10.1016/j.lithos.2020.105544.

References

Aulbach, S., Stagno, V., 2016. Evidence for a reducing Archean ambient mantle and its effects on the carbon cycle. Geology 44, 751–754.
Bekker, A., Holland, H.D., 2012. Oxygen overshoot and recovery during the early Paleoproterozoic. Earth Planet. Sci. Lett. 317, 295–304.
Bézoes, A., Humler, E., 2005. The $Fe^{3+}/\Sigma Fe$ ratios of MORB glasses and their implications for mantle melting. Geochim. Cosmochim. Acta 69, 711–725.
Brounce, M.N., Kelley, K.A., Cottrell, E., 2014. Variations in Fe^{3+}/Sigma Fe of Mariana Arc Basalts and Mantle Wedge fO_2. J. Petrol. 55, 2513–2536.
Brounce, M., Stolper, E., Eiler, J., 2017. Redox variations in Mauna Kea lavas, the oxygen fugacity of the Hawaiian plume, and the role of volcanic gases in Earth's oxygenation. Proc. Natl. Acad. Sci. U. S. A. 114, 8997–9002.
Canil, D., 2002. Vanadium in peridotites, mantle redox and tectonic environments, Archean to present. Earth Planet. Sci. Lett. 195, 75–90.
Cottrell, E., Kelley, K.A., 2011. The oxidation state of Fe in MORB glasses and the oxygen fugacity of the upper mantle. Earth Planet. Sci. Lett. 305, 270–282.
Cottrell, E., Kelly, K.A., 2013. Redox heterogeneity in Mid-ocean ridge basalts as a function of mantle source. Science 340, 1314–1317.
Danyushevsky, L.V., Plechov, P., 2011. Petrolog 3, integrated software for modeling crystallization processes. Geochem. Geophys. Geosyst. 12. https://doi.org/10.1029/2011GC003516.
Dasgupta, R., Hirschmann, M.M., Withers, A.C., 2004. Deep global cycling of carbon constrained by the solidus of anhydrous, carbonated eclogite under upper mantle conditions. Earth Planet. Sci. Lett. 227, 73–85.
Dasgupta, R., Hirschmann, M.M., Stalker, K., 2006. Immiscible transition from carbonate-rich to silicate-rich melts in the 3 GPa melting interval of eclogite + CO_2 and genesis of silica-undersaturated ocean island lavas. J. Petrol. 47, 647–671.
Dasgupta, R., Hirschmann, M.M., McDonough, W.F., Spiegelman, M., Withers, A.C., 2009. Trace element partitioning between garnet lherzolite and carbonatite at 6.6-8.6 GPa with applications to the geochemistry of the mantle and of mantle-derived melts. Chem. Geol. 262, 57–77.
de Moor, J.M., Fischer, T.P., Sharp, Z.D., King, P.L., Wilke, M., Botcharnikov, R.E., Cottrell, E., Zelenski, M., Marty, B., Klimm, K., Rivard, C., Ayalew, D., 2013. Sulfur degassing at Erta Ale (Ethiopia) and Masaya (Nicaragua) volcanoes: Implications for degassing processes and oxygen fugacities of basaltic systems. Geochemistry Geophysics Geosystems 14. https://doi.org/10.1002/ggge.20255.
Debret, B., et al., 2015. Redox state of iron during high-pressure serpentinite dehydration. Contrib. Mineral. Petrol. 169, 36.
Dsgupta, R., Hirshcmann, M.M., 2010. The deep carbon cycle and melting in Earth's interior. Earth Planet. Sci. Lett. 298, 1–13.
Eguchi, J., Dasgupta, R., 2018. Redox state of the convective mantle from CO_2-trace element systematics of oceanic basalts. Geochem. Perspect. Lett. 8, 17–21.
Evans, K.A., 2012. The redox budget of subduction zones. Earth Sci. Rev. 113, 11–32.
Frost, D.J., McCammon, C.A., 2008. The redox state of Earth's mantle. Ann. Rev. Earth Planet. Sci. 36, 389–420.
Gaillard, F., Malki, M., Iacono-Marziano, G., Pichavant, M., Scaillet, B., 2008. Carbonatite melts and electrical conductivity in the Asthenosphere. Science 322, 1363–1365.
Gu, Y.T., Lerner-Lamb, A.L., Dziewonskic, A.M., Ekström, G., 2005. Deep structure and seismic anisotropy beneath the East Pacific Rise. Earth Planet. Sci. Lett. 232, 259–272.
Gudmundsson, G., Wood, B.J., 1995. Experimental tests of garnet peridotite oxygen barometry. Contrib. Mineral. Petrol. 119, 56–67.
He, Y.S., Meng, X.N., Ke, S., Wu, H.J., Zhu, C.W., Teng, F.Z., Hoefs, J., Huang, J., Yang, W., Xu, L.J., Hou, Z.H., Ren, Z.Y., Li, S.G., 2019. A nephelinitic component with unusual $\delta^{56}Fe$ in Cenozoic basalts from eastern China and its implications for deep oxygen cycle. Earth Planet. Sci. Lett. 512, 175–183.
Herzberg, C., 2011. Identification of source lithology in the Hawaiian and Canary Islands, implications for origins. J. Petrol. 52, 113–146.
Herzberg, C., Asimow, P.D., 2008. Petrology of some oceanic island basalts: PRIMELT2.XLS software for primary magma calculation. Geochem. Geophys. Geosyst. 9. https://doi.org/10.1029/2008GC002057.
Hirschamnn, M.M., 2000. Mantle solidus: Experimental constraints and the effects of peridotite composition. Geochem. Geophys. Geosyst. 1. https://doi.org/10.1029/2000gc000070.
Hirschmann, M.M., 2018. Comparative deep Earth volatile cycles: The case for C recycling from exosphere/mantle fractionation of major (H2O, C, N) volatiles and from H2O/Ce, CO2/Ba, and CO2/Nb exosphere ratios. Earth and Planetary Science Letters 502, 262–273.
Hofmann, A.W., 1997. Mantle geochemistry: the message from oceanic volcanism. Nature 385, 219–229.
Huang, J.L., Zhao, D.P., 2006. High-resolution mantle tomography of China and surrounding regions. J. Geophys. Res. 111. https://doi.org/10.1029/2005JB004066.

Humphreys, M.C.S., Brooker, R.A., Fraser, D.G., Burgisser, A., Mangan, M.T., McCam-mon, C., 2015. Coupled interactions between volatile activity and Fe oxidation state during arc crustal processes. J. Petrol. 56, 795–814.
Karato, S.I., 2011. Water distribution across the mantle transition zone and its implications for global material circulation. Earth Planet. Sci. Lett. 301, 413–423.
Kelemen, P.B., Manning, C.E., 2015. Reevaluating carbon fluxes in subduction zones, what goes down, mostly comes up. PNAS 112, E3997–E4006.
Kelley, K.A., Cottrell, E., 2009. Water and the oxidation state of subduction zone magmas. Science 325, 605–607.
Kelley, K.A., Cottrell, E., 2012. The influence of magmatic differentiation on the oxidation state of Fe in a basaltic arc magma. Earth Planet. Sci. Lett. 329, 109–121.
Kerrick, D.M., Connolly, J.A.D., 2001. Metamorphic devolatilization of subducted mid-ocean ridge metabasalts: implications for seismicity, arc magmatism and volatile recycling. Earth Planet. Sci. Lett. 189, 19–29.
Kono, Y., Kenney-Benson, C., Hummer, D., Ohfuji, H., Park, C., Shen, G.Y., Wang, Y.B., Kavner, A., Manning, C.E., 2014. Ultralow viscosity of carbonate melts at high pressure. Nat. Commun. 5, 5091.
Kress, V., Carmichael, I.S.E., 1988. Stoichiometry of the Iron Oxidation Reaction in Silicate Melts. Am. Mineral. 73, 11–12.
Li, H.Y., Xu, Y.G., Ryan, J.G., Huang, X.L., Ren, Z.Y., Guo, H., Ning, Z.G., 2016. Olivine and melt inclusion chemical constraints on the source of intracontinental basalts from the eastern North China Craton: Discrimination of contributions from the subducted Pacific slab. Geochim. Cosmochim. Acta 178, 1–19.
Li, S.G., Yang, W., Ke, S., Meng, X.N., Tian, H.C., Xu, L.J., et al., 2017. Deep carbon cycles constrained by a large-scale mantle Mg isotope anomaly in eastern China. Natl. Sci. Rev. 4, 111–120.
Liu, Y.S., Gao, S., Kelemen, P.B., Xu, W.L., 2008. Recycled crust controls contrasting source compositions of Mesozoic and Cenozoic basalts in the North China Craton. Geochimica et Cosmochimica Acta 72, 2349–2376.
Liu, S.A., Wang, Z.Z., Li, S.G., Huang, J., Yang, W., 2016. Zinc isotope evidence for a large-scale carbonated mantle beneath eastern China. Earth Planet. Sci. Lett. 444, 169–178.
Lizarralde, D., Chave, A., Hirth, G., Schultz, A., 1995. Northeastern Pacific mantle conductivity profile from long-period magetotelluric sounding using Hawaii-to-California submarine cabe data. J. Geophys. Res. 100, 17837–17854.
Luo, D., Chen, L.-H., Zeng, G., 2009. Gensis of intra-continental strongly alkaline volcanic rocks: a case study of Dashan nephelinites in Wudi, Shandong Province. North China. Acta Petrologica Sinica 25, 311–319 (in Chinese with English abstract).
Mallmann, G., O'Neill, H., 2009. The crystal/melt partitioning of V during mantle melting as a function of oxygen fugacity compared with some other elements (Al, P, Ca, Sc, Ti, Cr, Fe, Ga, Y, Zr and Nb). Journal of Petrology 50, 1765–1794.
McKenzie, D., Jackson, J., Priestley, K., 2005. Thermal structure of oceanic and continental lithosphere. Earth Planet. Sci. Lett. 233, 337–349.
Moussallam, Y., Oppenheimer, C., Scaillet, B., Gaillard, F., Kyle, P., Peters, N., Hartley, M., Berlo, K., Donovan, A., 2014. Tracking the changing oxidation state of Erebus magmas, from mantle to surface, driven by magma ascent and degassing. Earth Planet. Sci. Lett. 393, 200–209.
Moussallam, Y., Edmonds, M., Scillet, B., Peters, N., Gennaro, E., Sides, I., Oppenheimer, C., 2016. The impact of degassing on the oxidation state of basaltic magmas: A case study of Kilauea volcano. Earth and Planetary Science Letters 450, 317–325.
Nicklas, R.W., Puchtel, I.S., Ash, R.D., Piccoli, P.M., Hanski, E., Nisbet, E.G., Waterton, P., Pearson, D.G., Anbar, A.D., 2019. Secular mantle oxidation across the Archean-Proterozoic boundary: evidence from V partitioning in komatiites and picrites. Geochim. Cosmochim. Acta 205, 49–75.
Niu, Y.L., 2005. Generation and evolution of basaltic magmas: some basic concepts and a new view on the origin of Mesozoic-Cenozoic basaltic volcanism in Eastern China. Geol. J. China Univ. 11, 9–46.
Rohrbach, A., Schmidt, M.W., 2011. Redox freezing and melting in the Earth's deep mantle resulting from carbon-iron redox coupling. Nature 472, 209–212.
Sakuyama, T., Tian, W., Kimura, J., Fukao, Y., Hirahara, Y., Takahashi, T., Senda, R., Chang, Q., Miyazaki, T., Obayashi, M., Kawabata, H., Tatsumi, Y., 2013. Melting of dehydrated oceanic crust from the stagnant slab and of the hydrated mantle transition zone: Constraints from Cenozoic alkaline basalts in eastern China. Chem. Geol. 359, 32–48.
Shaw, G.H., 2008. Earth's atmosphere-Hadean to early Proterozoic. Chemie der Erde- Geochemistry 68, 235–264.
Shorttle, O., Moussallam, Y., Hartley, M.E., Maclennan, J., Edmonds, M., Murton, B.J., 2015. Fe-Xanes analyses of Reykjanes Ridge basalts: Implications for oceanic crust's role in the solid Earth oxygen cycle. Earth Planet. Sci. Lett. 427, 272–285.
Sifré, D., Gardés, E., Massuyeau, M., Hashim, L., Hier-Majumder, S., Gaillard, F., 2014. Electrical conductivity during incipient melting in the oceanic low-velocity zone. Nature 509, 81–85.
Sobolev, A.V., Hofmann, A.W., Sobolev, S.V., Nikogosian, I.K., 2005. An olivine-free mantle source of Hawaiian shield basalts. Nature 434, 590–597.
Spandler, C., Yaxley, G., Green, D.H., Rosenthal, A., 2008. Phase relations and melting of anhydrous K-bearing eclogite from 1200-1600°C and 3 to 5 GPa. J. Petrol. 49, 771–795.
Stagno, V., Ojwang, D.O., McCammon, C.A., Frost, D.J., 2013. The oxidation state of the mantle and the extraction of carbon from Earth's interior. Nature 493, 84–88.
Stagno, V., Frost, D.J., McCammon, C.A., Mohseni, H., Fei, Y., 2015. The oxygen fugacity at which graphite or diamond forms from carbonate-bearing melts in eclogitic rocks. Contrib. Mineral. Petrol. 169. https://doi.org/10.1007/s00410-015-1111-1.
Sun, C.G., Dasgupta, R., 2019. Slab-mantle interaction, carbon transport and kimberlite generation in the deep upper mantle. Earth Planet. Sci. Lett. 506, 38–52.
Takahashi, E., Nakajima, K., Wright, T.L., 1998. Origin of the Columbia River basalts: melting model of a heterogeneous plume head. Earth Planet. Sci. Lett. 162, 63–80.
Teng, F.Z., Li, W.Y., Ke, S., et al., 2010. Magnesium isotopic composition of the Earth and chondrites. Geochim. Cosmochim. Acta 74, 5039–5053.
Thomson, A.R., Walter, M.J., Kohn, S.C., Brooker, R.A., 2016. Slab melting as a barrier to deep carbon subduction. Nature 529, 76–79.
Van Hunen, J., Moyen, J.F., 2012. Archean subduction: Fact or fiction? Ann. Rev. Earth Planet. Sci. 40, 195–219.
Wang, Z.Z., Liu, S.A., Liu, J., Huang, J., Xiao, Y., Chu, Z.Y., Zhao, X.M., Tang, L., 2017. Zinc isotope fractionation during mantle melting and constrains on the Zn isotope composition of Earth's upper mantle. Geochim. Cosmochim. Acta 198, 151–167.
Wang, Z.Z., Liu, S.A., Chen, L.H., Li, S.G., Zeng, G., 2018. Compositional transition in natural alkaline lavas through silica-undersaturated melt-lithosphere interaction. Geology 46, 771–774.
White, W.M., 2010. Oceanic island basalts and mantle plumes: the geochemical perspective. Ann. Rev. Earth Planet. Sci. 38, 133–160.
Xu, Y.G., 2014. Recycled oceanic crust in the sources of 90-40Ma basalts in North and Northeast China: evidence, provenance and significance. Geochim. Cosmochim. Acta 143, 49–67.
Xu, Y.G., Zhang, H.H., Qiu, H.N., Ge, W.C., Wu, F.Y., 2012. Oceanic crust components in continental basalts from Shuangliao, Northeast China: Derived from the mantle transitional zone? Chem. Geol. 328, 168–184.
Xu, Y.G., Li, H.Y., Hong, L.B., Ma, L., Ma, Q., Sun, M.D., 2018. Generation of Cenozoic intraplate basalts in the big mantle wedge under eastern Asia. Sci. China Earth Sci. 61, 869–886.
Yang, Z.F., Zhou, J.H., 2013. Can we identify source lithology of basalt? Sci. Rep. 3. https://doi.org/10.1038/srep01856.
Zeng, G., Chen, L.H., Xu, X.S., Jiang, S.Y., Hofmann, A.W., 2010. Carbonated mantle sources for Cenozoic intra-plate alkaline basalts in Shandong, North China. Chem. Geol. 273, 35–45.
Zeng, G., Chen, L.H., Hofmann, A.W., Jiang, S.Y., Xu, X.S., 2011. Crust recycling in the source of two parallel volcanic chains in Shandong, North China. Earth and Planetary Science Letters 302, 359–368.
Zhang, L., Ren, Z.Y., Xia, X.P., Yang, Q., Hong, L.B., Wu, D., 2019. In situ determination of trace elements in melt inclusions using laser ablation-inductively coupled plasma-sector field-mass spectrometry. Rapid Commun. Mass Spectrom. https://doi.org/10.1002/rcm.8359.